Spatial hole burning in thin-disk lasers and twisted-mode operation

K. Schuhmann,[1,2,*] **K. Kirch,**[1,2] **F. Nez,**[3] **R. Pohl,**[4,5] **G. Wichmann,**[1] **and A. Antognini**[1,2]

[1]*Institute for Particle Physics and Astrophysics, ETH, 8093 Zurich, Switzerland*
[2]*Paul Scherrer Institute, 5232 Villigen PSI, Switzerland*
[3]*Laboratoire Kastler Brossel, Sorbonne Université, CNRS, ENS-PSL University, Collège de France 4 place Jussieu, 75005 Paris, France*
[4]*Johannes Gutenberg-Universität Mainz, QUANTUM, Institut für Physik & Exzellenzcluster PRISMA, 55099 Mainz, Germany*
[5]*Max-Planck-Institute for Quantum Optics, 85748 Garching, Germany*
*Corresponding author: skarsten@phys.ethz.ch

Spatial hole burning prevents single-frequency operation of thin-disk lasers when the thin disk is used as a folding mirror. We present an evaluation of the saturation effects in the disk for disks acting as end mirrors and as folding mirrors, explaining one of the main obstacles toward single-frequency operation. It is shown that a twisted-mode scheme based on a multi-order quarter-wave plate combined with a polarizer provides an almost complete suppression of spatial hole burning and creates an additional wavelength selectivity that enforces efficient single-frequency operation. © 2018 Optical Society of America

OCIS codes: (140.0140) Lasers and laser optics; (140.3615) Lasers, ytterbium; (070.2615) Frequency filtering; (140.3425) Laser stabilization.

https://doi.org/10.1364/AO.57.002900

1. INTRODUCTION

The various longitudinal modes of a laser cavity undergoing optical amplification in the same active medium experience the phenomenon of gain competition, which leads to the prevailing of one mode over all the others and thus to single-frequency operation [1]. A tiny difference of the effective gain seen by a mode is sufficient to initiate this prevailing process. However, the domination of one mode over all the others can be sustained only when the stimulated emission induced by this mode causes gain saturation not only for itself (self-saturation), but with equal strength also for the other modes (cross saturation). This cross saturation occurs when the amplification of the various modes addresses the same regions of the active medium, so that the amplification of one mode depletes also the population inversion experienced by the other modes. If the various modes address the distribution of the population inversion in different ways, as in the case of "spatial hole burning" (SHB) [1,2], the amplification process of one mode only partially affects the population inversion experienced by the other modes. Several modes can thus coexist in steady-state conditions in a linear laser cavity preventing single-frequency operation.

The principle of SHB and its relation to single-frequency operation is illustrated in Fig. 1. In the center of a linear cavity, the standing wave pattern of the 14th longitudinal mode (black continuous curves) has maxima where the 13th longitudinal

mode (black dashed curves) has minima. Therefore, the depletion of the population inversion caused by the 14th mode reduces the gain of the 14th mode (self-saturation) but does not significantly decrease the gain of the 13th mode (negligible cross saturation). As a consequence, the gain competition between these two adjacent longitudinal modes is strongly suppressed, and the laser operates simultaneously in several longitudinal modes.

SHB is often eliminated by the use of unidirectional ring-laser cavities. However, this is not an option for high-power thin-disk lasers, as Faraday rotators, required to enforce the unidirectional operation, lack the power-handling capability [3]. A well-established method to eliminate SHB in a linear cavity is given by the so-called twisted-mode scheme [1,4–7] where the counter-propagating beams in the active medium have orthogonal polarizations so that no interference occurs. To our knowledge, this method has so far not been applied to thin-disk lasers, except in our previous work [8].

By reducing the length of a laser cavity (in the micrometer range for Yb:YAG as active medium), the effect of SHB in preventing single-frequency operation can be eliminated. Indeed for such a short cavity, only one longitudinal mode falls into the spectral region where the active medium has a gain. Yet, these short cavities are not apt for high-power lasers, as they cannot sustain modes with large transverse size. Wavelength selective elements as gratings or Fabry–Perot etalons could
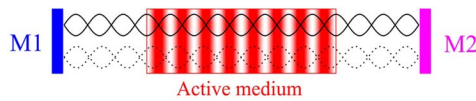
Fig. 1. Scheme illustrating the principle of SHB in the active medium of a linear laser cavity. The end mirrors (M1 and M2) are given in blue and magenta, respectively. The continuous black curves show the envelope of the time varying amplitude of a cavity mode saturating the active medium. The red color represents the position-dependent population inversion in the active medium caused by gain saturation of this mode. The dashed black curves show the envelope of one neighboring mode. This mode experiences additional gain as it addresses portions of the active medium that are not strongly saturated by the first mode. Thus, both modes can coexist in the cavity.

be used to favor one of the modes, but also in these cases, an efficient selectivity can be achieved only for relatively short cavity lengths.

Another method to suppress the disrupting effects of SHB and to achieve single-frequency operation is obtained by using a short active medium placed close to a cavity end mirror. This is often called a "gain-at-the-end" configuration. In fact, as can be deduced from Fig. 1, in this region, the intensity maxima of neighboring modes are located at similar positions so that these modes sample the active medium with nearly identical patterns. Thus, a strong cross saturation between neighboring modes exists, which leads to the prevailing of the dominant mode over the others. Because of this, a thin-disk laser with the disk acting as end-mirror M1 is suitable for high-power lasers in single-frequency operation given the mitigation of the effects of SHB and the power scalability of the thin disk [8–10].

Improper understanding of the "gain-at-the-end" configuration has sometimes led to erroneously neglecting SHB when the thin disk is used as a folding mirror of the resonator. In such a case, the SHB pattern is more complex than presented in Fig. 1 because it results from the interference of four circulating beams, as recognized by Vorholt and Wittrock in Ref. [11]. However, their model does not include the dependence on the distance between the active medium and the end mirror (see D_3 in Fig. 9). SHB for disks acting as folding mirrors has also been discussed for mode-locked lasers [12,13], though this is not applicable for continuous wave (cw) and ns pulses. This study aims to clarify the SHB effects taking place in thin-disk lasers and their relation to single-frequency operation.

In Section 2 we introduce the fundamentals of SHB for the simple situation presented in Fig. 1, similar to the studies in Refs. [14–16]. The obtained results are then applied in Section 3 to the case of thin-disk lasers with the thin disk acting as cavity end mirror. In this design, SHB favors longitudinal modes with a large frequency spacing from the lasing (saturating) mode, which can be easily suppressed using standard frequency selective elements. Section 4 presents SHB when the thin disk acts as a folding mirror. The resulting interference of four beams in the active medium increases the susceptibility for SHB. In Section 5, we apply the twisted-mode scheme [4–7] to this cavity layout to reduce the four-beam to a two-beam interference, nearly eliminating the SHB. It is

concluded with Section 6 presenting an implementation of the twisted-mode scheme in a Q-switched thin-disk laser [17].

2. SPATIAL HOLE BURNING FOR A LINEAR CAVITY

In this section, the well-known principle of SHB is derived for the linear cavity in Fig. 2 by using the generic building block of an amplifier given in Fig. 3. In this amplifier, a saturating Gaussian beam at a wavelength λ_0 passes an active medium and travels to a mirror M1, which is reflecting the beam back onto itself. Thus, the beam crosses the medium a second time. The origin of the coordinate system used to compute SHB is located in the center of the active medium with z the propagation and x, y the transverse directions. The position- and time-dependent amplitude of the forward propagating beam inside the active medium ($z \in [-L/2, +L/2]$ with the length of the active medium L) can be written as

$$E_1(x, y, z, t, \lambda_0) = E_0 \cos\left(2\pi\left(-\frac{nz}{\lambda_0} - \nu_0 t\right)\right)$$
$$\cdot \exp\left(-\frac{x^2 + y^2}{2w^2}\right), \quad \textbf{(1)}$$

with w the width of the transverse profile of the beam, n the refractive index of the active medium, t the time, E_0 the amplitude of the beam on its symmetry axis, and ν_0 and $\lambda_0 = c/\nu_0$ the frequency and wavelength of the beam, respectively. For simplicity, we neglected the increase of amplitude occurring in the active medium. This simplification allows for analytical results and is well justified for low-gain media as the thin disk. Furthermore, it provides qualitatively valid results also for high-gain media. Note that the laser gain will be accounted for separately [see, e.g., Eq. (9)]. The corresponding backward propagating beam is given by
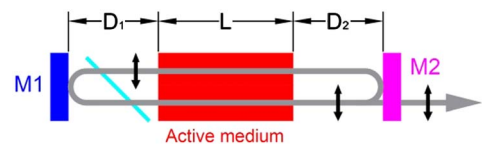
Fig. 2. Scheme of a linear cavity with active medium (red), end mirrors (M1 and M2) (blue and magenta) and polarizer (cyan). The black arrows indicate the beam polarization.
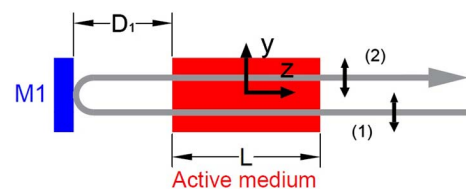
Fig. 3. Scheme of a dual-pass amplifier used to evaluate the SHB also for the linear cavity in Fig. 2. Same color convention is used as in Fig. 2. Due to the absence of resonant condition, the possible values of λ and λ_0 are not constrained.

$$E_2(x,y,z,t,\lambda_0) = E_0 \cos\left(2\pi\left(\frac{2d+nz}{\lambda_0} - \nu_0 t\right)\right)$$
$$\cdot \exp\left(-\frac{x^2+y^2}{2w^2}\right), \tag{2}$$

where $d = D_1 + nL/2$ is the optical distance between the center of the active medium and M1 with D_1 the distance between the active medium and M1 (cf. Figs. 1 and 3). The total amplitude in the active medium resulting from the superposition of the two beams is thus

$$E(x,y,z,t,\lambda_0) = E_1 + E_2$$
$$= 2E_0 \cos\left(2\pi\left(\frac{d}{\lambda_0} - \nu_0 t\right)\right) \cos\left(2\pi\frac{d+nz}{\lambda_0}\right)$$
$$\cdot \exp\left(-\frac{x^2+y^2}{2w^2}\right). \tag{3}$$

The position dependency of the time-averaged intensity distribution resulting from the two counter-propagating beams is given by

$$I(x,y,z,\lambda_0) = 2I_0\left(1 + \cos\left(4\pi\frac{nz+d}{\lambda_0}\right)\right)\exp\left(-\frac{x^2+y^2}{w^2}\right), \tag{4}$$

where $I_0 = cn\varepsilon_0|E_0^2|/2$ is the intensity of a single laser beam on its symmetry axis. From this intensity distribution $I(x,y,z,\lambda_0)$, it is possible to obtain the position-dependent density of the population inversion in the active material $N(x,y,z,\lambda_0)$ by using the known rate equation for a four-level laser [1]:

$$\frac{dN(x,y,z,t,\lambda_0)}{dt} = R_p - N(x,y,z,t,\lambda_0)\frac{I(x,y,z,t,\lambda_0)}{F_{sat}}$$
$$- \frac{N(x,y,z,t,\lambda_0)}{\tau}, \tag{5}$$

where R_p is the pump rate (homogeneous within the active medium), F_{sat} the saturation fluence, and τ the lifetime of the upper state. The decrease of the upper state population by the stimulated emission is proportional to the local intensity of the circulating light $I(x,y,z,\lambda_0)$. The steady-state solution of this rate equation ($dN/dt = 0$) reads

$$N(x,y,z,\lambda_0) = \frac{R_p\tau}{1 + \tau\frac{I(x,y,z,\lambda_0)}{F_{sat}}}, \tag{6}$$

$$\approx R_p\tau - R_p\tau^2\frac{I(x,y,z,\lambda_0)}{F_{sat}} + \mathcal{O}(I^2). \tag{7}$$

In Eq. (7), we assumed that $\tau\frac{I(x,y,z,\lambda_0)}{F_{sat}} \ll 1$, which is valid for a weakly saturating beam intensity, e.g., for a laser cavity with an out-coupling mirror of low reflectivity. (For efficient laser operation, high saturation of the active medium is required. In this case, this assumption does not hold. Nevertheless, the general behavior presented in this study remains valid).

The position-dependent gain $g(x,y,z,\lambda_0)$ is proportional to the local density of the population inversion and can be expressed as

$$g(x,y,z,\lambda_0) \approx g_0 - g_0\tau\frac{I(x,y,z,\lambda_0)}{F_{sat}}, \tag{8}$$

where g_0 is the unsaturated gain.

So far, we have described the SHB effect of the dominant laser beam with a wavelength λ_0 amplified in a dual-pass configuration, as depicted in Fig. 3. As a next step, we evaluate the saturation spectrum of the active medium experienced by a second (probing) beam at a wavelength λ. This beam forms a similar interference pattern $I(x,y,z,\lambda)$ in the active medium slightly shifted relative to $I(x,y,z,\lambda_0)$. The cross-saturation gain G experienced by this beam is given by the integral

$$G(\lambda) = \frac{\iiint I(x,y,z,\lambda)g(x,y,z,\lambda_0)dxdydz}{P_{laser}}, \tag{9}$$

where P_{laser} is the incident laser power at wavelength λ_0. The gain G can be described as the product of the unsaturated laser gain G_0 and the saturation spectrum $S_{SHB}(\lambda)$, so that the output power is

$$P_{out} = e^{G(\lambda)}P_{in} = e^{S_{SHB}(\lambda)G_0(\lambda)}P_{in}. \tag{10}$$

The saturation spectrum $S_{SHB}(\lambda)$ for the dual-pass configuration of Fig. 3 is thus given by

$$S_{SHB}(\lambda) = \frac{G}{G_0} = \frac{\int_{-\infty}^{\infty}\int_{-\infty}^{\infty}\int_{-L/2}^{L/2} I(x,y,z,\lambda)g(x,y,z,\lambda_0)dzdxdy}{\int_{-\infty}^{\infty}\int_{-\infty}^{\infty}\int_{-L/2}^{L/2} I(x,y,z,\lambda)g_0 dzdxdy}. \tag{11}$$

Combining Eq. (8) with Eq. (11), we find

$$S_{SHB}(\lambda) = 1 - \frac{\tau}{I_0 F_{sat} L}\int_{-\infty}^{\infty}\int_{-\infty}^{\infty}\int_{-L/2}^{L/2} I(x,y,z,\lambda_0)$$
$$\cdot I(x,y,z,\lambda)dzdxdy. \tag{12}$$

Inserting the time-averaged intensity of Eq. (4) into Eq. (12), and assuming that d and L are much larger than λ and λ_0, and also that $\Delta \equiv (\lambda_0 - \lambda)/(\lambda_0\lambda) \ll 1/\lambda_0$, we find

$$S_{SHB}(\lambda) \approx 1 - 2\frac{\tau I_0}{F_{sat}}\left(1 + \frac{1}{2}\text{sinc}(\pi nL\Delta)\cos(2\pi d\Delta)\right). \tag{13}$$

To obtain this result, we have made use of the approximation

$$\int_{-L/2}^{L/2}\left(1 + \cos\left(2\pi\frac{nz+d}{\lambda_0}\right)\right)\left(1 + \cos\left(2\pi\frac{nz+d}{\lambda}\right)\right)dz$$
$$\approx L\left(1 + \frac{1}{2}\text{sinc}(\pi nL\Delta)\cos(2\pi d\Delta)\right).$$

A plot of the saturation spectrum $S_{SHB}(\lambda)$ for realistic values of d and L is shown in Fig. 4 as a function of the wavelength λ of the probe beam assuming a saturating beam at $\lambda_0 = 1030$ nm. When applying these results to a cavity, it is necessary to take into account that the wavelengths λ and λ_0 can have discrete values only as a consequence of the resonance conditions. For the simplified cavity layout in Fig. 2 with $D_1 = D_2$, the longitudinal modes neighboring the saturating mode are located exactly at the two maxima of $S_{SHB}(\lambda)$, as indicated by the blue hollow circles in Fig. 4. These two modes
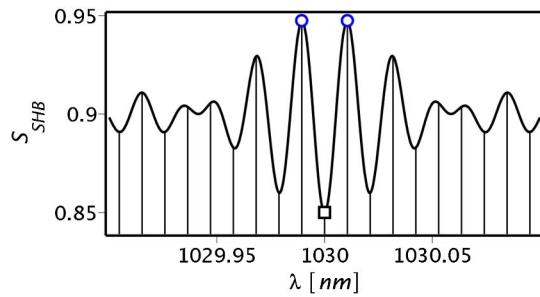
Fig. 4. Saturation spectrum S_{SHB} of the amplifier given in Fig. 3 computed with Eq. (13) assuming $D_1 = 40$ mm, $L = 10$ mm, $2\tau I_0 / F_{\mathrm{sat}} = 10\%$, and the saturating wavelength $\lambda_0 = 1030$ nm. The plot also represents S_{SHB} of the linear cavity in Fig. 2 with $D_1 = D_2 = 40$ mm. The vertical lines indicate the wavelength of the cavity eigenmodes. The gain experienced by the saturating mode is indicated by the black empty square, the gain experienced by its neighboring modes by the empty blue circles.

experience thus a gain decrease due to saturation effects significantly smaller compared to the gain decrease at the saturating wavelength λ_0. Therefore, amplification of these neighboring modes occurs leading to disruption of single-frequency operation. Because the spectral distance between modes for realistic layouts of rod lasers with typical cavity round-trip length of about 0.1 m is 1.5 GHz (5 pm at 1030 nm), the suppression of the neighboring modes using selective elements would require extremely narrow spectral filters with active regulation to prevent significant cavity losses at the operating wavelength λ_0.

3. SPATIAL HOLE BURNING FOR A THIN DISK ACTING AS CAVITY END MIRROR

For a thin disk acting as a cavity end-mirror M1 (see Fig. 5), the effects related with SHB are mitigated. Indeed for this "gain-at-the-end" configuration, the intensity pattern in the active medium (see Fig. 6) changes so slowly with the wavelength λ that the maxima and minima of the intensity pattern of two neighboring axial cavity modes are located at similar positions (cf. Fig. 1). This implies that the cross saturation between neighboring modes is nearly identical to the self-saturation. In other words, the saturation spectrum $S_{\mathrm{SHB}}(\lambda)$ is a slowly varying function of λ.

The reduction of gain caused by the saturation spectrum $S_{\mathrm{SHB}}(\lambda)$ for thin-disk lasers with disks acting as cavity end-mirrors can be quantified using Eq. (13) and setting $D_1 = 0$ (cf. Figs. 2 with 5):
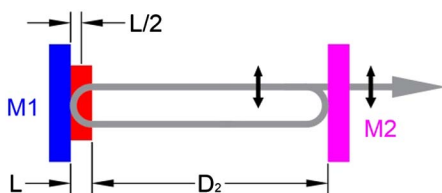
Fig. 5. Scheme of a thin-disk cavity where the disk is acting also as end-mirror M1. Same color code as in Fig. 2.
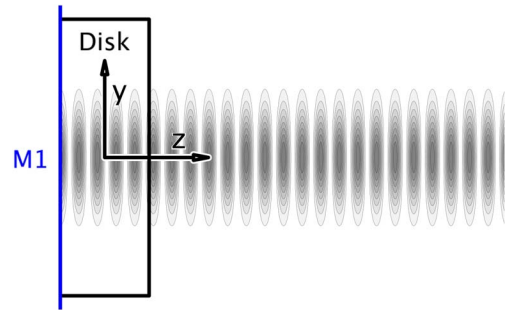
Fig. 6. Intensity pattern in the disk when the back side of the disk is reflecting the beam in itself. Due to the two-beam interference, the maximal intensity is $4I_0$. The boundary conditions at mirror M1 impose the interference pattern to have an anti-node at the M1 position. Therefore, the positions of the maxima and minima of the interference pattern change slowly with the wavelength λ.

$$S_{\mathrm{SHB}}(\lambda) \approx 1 - 2\frac{\tau I_0}{F_{\mathrm{sat}}}\left(1 + \frac{1}{2}\mathrm{sinc}(\pi n L \Delta)\right). \quad \textbf{(14)}$$

S_{SHB} is plotted in Fig. 7 as a function of the wavelength λ for a realistic thin-disk laser ($D_2 = 2$ m) having a saturating mode at $\lambda_0 = 1030$ nm. A long cavity was assumed in this case to provide an intra-cavity beam with large w required for the high-power operation. Because of this, the wavelength difference between neighboring modes in the 1030 nm region is only about 0.25 pm (75 MHz) apart, as indicated by the vicinity of the blue hollow circles and the black hollow square in Fig. 7(b). Thus, competition between the various modes located around the broad minimum centered at 1030 nm exists, which can be used to achieve single-frequency operation. In Fig. 7(a), the red squares indicate the maxima of the saturation spectrum S_{SHB} at a spectral distance of 2.11 nm (615 GHz) from λ_0. These modes could grow in the laser cavity and disrupt single-frequency operation. However, due to the large spectral distance of these maxima, the laser operation at these wavelengths can be easily suppressed by introducing a standard frequency selective element (e.g., a birefringent filter or a grating [18]) without active stabilization.

4. SPATIAL HOLE BURNING FOR A THIN DISK AS A FOLDING MIRROR

A more stable output beam for variations of the thin-disk thermal lens can be obtained by using the thin disk as a folding mirror in a V-shaped cavity (see Fig. 8). The stability properties of a laser containing a thermal lens have been studied in [19]. The thermal lens splits the cavity into two parts. The part that is longer (effective length given by the B-element of the corresponding ABCD matrix) has a complex beam parameter q that exhibits a linear (first-order) dependence on variations of the thermal lens. By contrast, the q-parameter in the shorter part exhibits a second-order dependence on variations of the thermal lens around the center of stability. Thus, to minimize variations of size and divergence of the output beam, the out-coupling mirror has to be placed in the short part of the cavity. When the thin disk is used as an end mirror of the cavity, it would be necessary to use the rear side of the disk as an

(a)

(b)
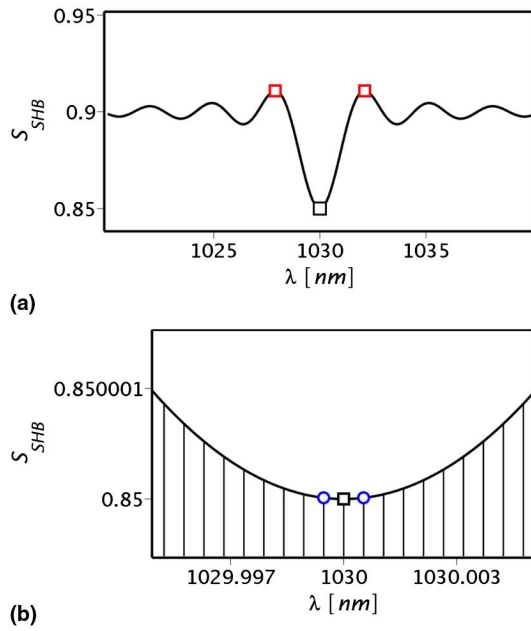
Fig. 7. (a) Saturation spectrum S_{SHB} of a thin disk caused by a beam reflected at the disk rear side as a function of the wavelength λ calculated using Eq. (14). The saturating mode is at $\lambda_0 = 1030$ nm, $D_1 = 0$ m, $L = 0.4$ mm, $w = 1$ mm, and $2\tau I_0 / F_{\text{sat}} = 10\%$. The self-saturation is indicated by the black empty square. The red empty squares indicate the spectral position of minimal cross saturation. (b) Zoom by a factor of 2×10^4 of the plot in panel (a) around the saturating wavelength. The vertical lines indicate the wavelengths of the eigenmodes for the cavity of Fig. 5, assuming $D_2 = 2$ m. The cross saturation of the neighboring modes, which is indicated by the empty blue circles, is nearly identical to the self-saturation.

out-coupling mirror, which is not feasible. As a result, the beam out-coupled from a thin-disk laser with the disk acting as end mirror suffers from a large sensitivity to variations of the thermal lens of the active medium. On the contrary, in a V-shaped cavity, the disk is used as a folding mirror, and the out-coupling mirror can be placed in the short (stable) part of the cavity leading to an out-coupled beam insensitive to variations of the thermal lens [8].

In contrast to the simple linear cavity of Fig. 5, in the V-shaped cavity with the disk acting as folding-mirror M1, the consideration of the SHB requires the evaluation of the
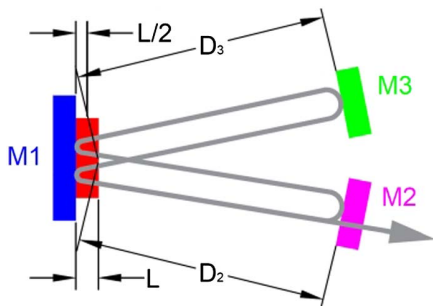
Fig. 8. Scheme of a thin-disk cavity with V-shaped layout where the disk is acting as folding-mirror M1. The active medium is given in red, the end-mirrors M2 and M3 in green and magenta, respectively.
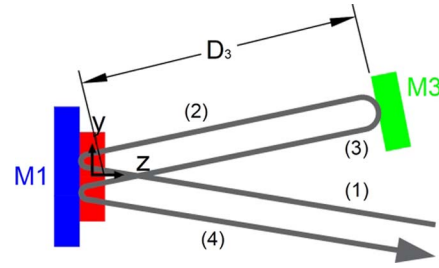
Fig. 9. Scheme of a four-pass thin-disk amplifier used to evaluate the SHB occurring in the active medium of the thin-disk cavity of Fig. 8 with V-shaped layout. The same color code as in Fig. 8 is used. Also indicated are the reference system and the four beams with amplitudes: E_1, E_2, E_3, and E_4.

interference of four beams similar to what was presented in [11]. Following the same methodology of Section 2 to compute the interference pattern, we proceed first by omitting M2 and computing the interference of the four beams for the amplifier configuration shown in Fig. 9. In a second step, the other end mirror (M2) is considered: it provides the resonance condition for the cavity.

The amplitude of the first beam $E_1(x, y, z, t, \lambda_0)$ traveling within the active medium with refractive index n from the disk front side toward the disk rear side can be described as

$$E_1(x, y, z, t, \lambda_0) = E_0$$
$$\cdot \cos\left(2\pi \frac{-nz\cos(\alpha) + ny\sin(\alpha)}{\lambda_0} - 2\pi\nu_0 t\right)$$
$$\cdot \exp\left(-\frac{x^2 + ((z+L/2)\sin(\alpha) - y\cos(\alpha))^2}{2w^2}\right),$$

$$(15)$$

where α is the propagation angle relative to the disk normal within the active medium. Again, we assume that the origin of the reference system is located at the center of the disk, thus at a distance $L/2$ from the disk's rear and front sides. The second beam originates from the reflection on the high-reflection (HR) coating at the rear side of the disk (M1). Within the active medium, the amplitude of this second beam $E_2(x, y, z, t, \lambda_0)$ is given by

$$E_2(x, y, z, t, \lambda_0) = E_0$$
$$\cdot \cos\left(2\pi \frac{(L+z)n\cos(\alpha) + ny\sin(\alpha)}{\lambda_0} - 2\pi\nu_0 t\right)$$
$$\cdot \exp\left(-\frac{x^2 + ((z+L/2)\sin(\alpha) + y\cos(\alpha))^2}{2w^2}\right).$$

$$(16)$$

A phase delay and an inversion of the propagation in z direction has been used to obtain this second beam from the first one, while size and direction in x and y directions are unchanged. This beam travels to M3 (given in green in Fig. 9), which reflects the beam in itself (inversion of all three propagation directions) back toward the active medium. The amplitude of this back-reflected beam traveling in the active medium from the front side to the rear side takes the form

$$E_3(x, y, z, t, \lambda_0) = E_0$$
$$\cdot \cos\left(2\pi \frac{2d + n(L - z)\cos(\alpha) - ny\sin(\alpha)}{\lambda_0} - 2\pi\nu_0 t\right)$$
$$\cdot \exp\left(-\frac{x^2 + ((z + L/2)\sin(\alpha) - y\cos(\alpha))^2}{2w^2}\right), \tag{17}$$

where $d = D_3 + nL/2$ is the optical distance between the active medium center and M3, with D_3 and L as defined in Fig. 9.

After a second reflection on the HR coating of the disk, a fourth beam moving from the disk rear side to the front side is ensued whose amplitude takes the form

$$E_4(x, y, z, t, \lambda_0) = E_0$$
$$\cdot \cos\left(2\pi \frac{2d + (2L + z)n\cos(\alpha) - ny\sin(\alpha)}{\lambda_0} - 2\pi\nu_0 t\right)$$
$$\cdot \exp\left(-\frac{x^2 + ((z + L/2)\sin(\alpha) + y\cos(\alpha))^2}{2w^2}\right). \tag{18}$$

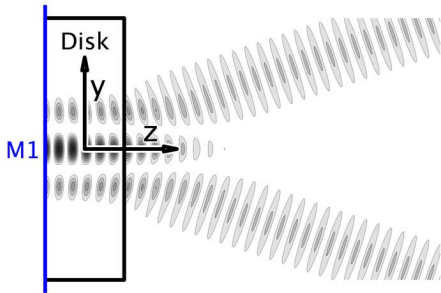The time-averaged intensity distribution resulting from the interference of the four traveling waves takes the form

$$I(x, y, z, \lambda_0) = 4I_0\left(1 + \cos\left(4\pi \frac{nz\cos(\alpha) + L/2}{\lambda_0}\right)\right)$$
$$\cdot \left(1 + \cos\left(4\pi \frac{ny\sin(\alpha) + d}{\lambda_0}\right)\right)\exp\left(-\frac{x^2 + y^2}{w^2}\right), \tag{19}$$

when walk-off effects are neglected. This approximation is justified given the small thickness of the disk ($L < 0.5$ mm) relative to the typical size of the cavity eigenmodes ($w > 1$ mm) and the small angle ($\alpha < 5°$).

An example of such an intensity pattern is shown in Fig. 10. By inserting Eq. (19) into Eqs. (8) and (11), the gain decrease related to the saturation effects is obtained:

$$S_{SHB}(\lambda) \approx 1 - 4\frac{\tau I_0}{F_{sat}}\left(1 + \frac{1}{2}\text{sinc}(\pi n L\Delta \cos(\alpha))\right)$$
$$\cdot \left(1 + \frac{1}{2}\cos(4\pi\Delta d)\exp(-2\Delta^2\pi^2 n^2 w^2\sin^2(\alpha))\right). \tag{20}$$

The saturation spectrum $S_{SHB}(\lambda)$ for $D_3 = 1$ m and $\alpha = 4.5°$ is shown in Fig. 11(a) as a function of the probe beam wavelength λ. The self saturation is depicted by the black square. The gray shaded region in the spectral plot of S_{SHB} represents rapid oscillations caused by the large optical distance D_3 between the active medium and the end-mirror M3. These rapid oscillations are visible in Fig. 11(b), where the horizontal axis is magnified by a factor of 2×10^4 in the wavelength region around the saturating wavelength $\lambda_0 = 1030$ nm. In the corresponding cavity ($D_3 = D_2 = 1$ m), the modes (indicated by the blue empty circles) nearest the saturating mode experience the maximal values of S_{SHB}. As the two neighboring modes (and others) have a larger small-signal gain, they will grow until they significantly contribute to the saturation of the gain medium. Hence, single-frequency operation is disrupted. Also in this case, a suppression of these modes would require an extremely narrow-band filter with active stabilization to prevent significant losses at the wavelength of the saturating mode.

5. TWISTED-MODE OPERATION OF A V-SHAPED THIN-DISK LASER

The twisted-mode scheme [4–7] represents a well-known possibility to eliminate SHB. Its principle is to insert two quarter-wave plates, one before and one after the active medium, as presented in Fig. 12(a), such that there is no interference in the active medium, because the two counter-propagating beams have orthogonal polarizations. The absence of the interference between the two circulating beams leads to the complete elimination of the SHB paving the way for single-frequency operation [20–23].

The twisted-mode scheme could be implemented also for thin-disk lasers with V-shaped cavities, as shown, e.g., in Fig. 12(b). Yet, contrary to the cavity of Fig. 12(a), in this case, the twisted-mode scheme does not completely eliminate the interference. The interference between the beams traveling
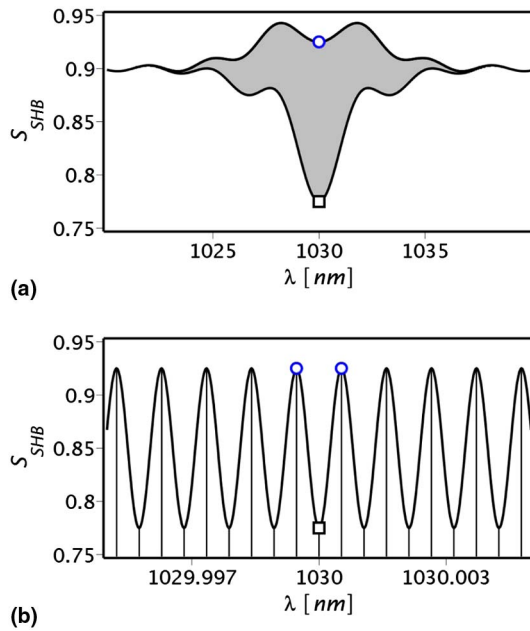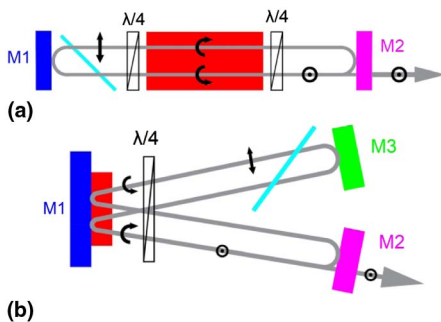
Fig. 10. Intensity pattern in the disk for a disk acting as a folding mirror in a V-shaped cavity. Due to the four-beam interference, the peak intensity is $16I_0$. This pattern results from the interference of four Gaussian beams in the configuration of Fig. 9. Because of the non-normal incidence within the thin disk, longitudinal and transversal interference patterns appear as described by Eq. (19).

Fig. 11. (a) Saturation spectrum $S_{SHB}(\lambda)$ of the 4-pass thin-disk amplifier from Fig. 9 calculated using Eq. (20) and assuming a saturating beam at $\lambda_0 = 1030$ nm, $D_3 = 1$ m, $L = 0.4$ mm, $\alpha = 4.5°$, $w = 1$ mm, and $4\tau I_0/F_{sat} = 10\%$. The gain experienced by the saturating beam is indicated by the black empty square. The gray shaded region represents rapid (unresolved) oscillations. (b) Zoom in by a factor of 2×10^4 around the saturating wavelength to present the fast oscillations of the $S_{SHB}(\lambda)$. The vertical lines indicate the possible wavelengths of the cavity eigenmodes given in Fig. 8 with $D_2 = D_3 = 1$ m.

to, and being back-reflected from, mirror M1 (rear side of the disk) cannot be eliminated. The resulting interference pattern, which is shown in Fig. 13, reduces thus from a four-beam to a two-beam interference, similar to Fig. 6.

This reduction of the four-beam interference to a two-beam interference can be seen in the mathematical expression of the saturation spectrum $S_{SHB}(\lambda)$, which takes the form

Fig. 12. (a) Linear cavity with a twisted-mode scheme obtained by inserting two quarter-wave plates around the active medium (red). (b) Cavity of a V-shaped thin-disk laser with a twisted-mode scheme obtained using only one multi-order quarter-wave plate. The polarization of the circulating beams is given by the black arrows and circles; the polarizer is in cyan.
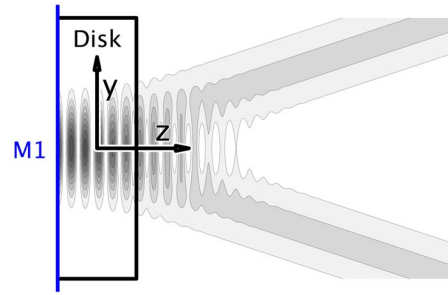
Fig. 13. Intensity pattern in the disk for a disk acting as a folding mirror in a V-shaped cavity and twisted-mode scheme as in Fig. 12(b). The twisted-mode scheme reduces the interference pattern of the four Gaussian beams shown in Fig. 9 to a two-beam interference (cf. to Fig. 10), resulting in a maximal intensity of $8I_0$. The interferences between E_1 and E_4 and between E_2 and E_3 are suppressed, while they are unchanged between E_1 and E_2 and between E_3 and E_4.

$$S_{SHB}(\lambda) \approx 1 - 4\frac{\tau I_0}{F_{sat}}\left(1 + \frac{1}{2}\text{sinc}(\pi n L \cos(\alpha)\Delta)\right), \quad \textbf{(21)}$$

similar to Eq. (14). This equation also represents the saturation spectrum for a unidirectional ring cavity, provided that $4I_0$ is substituted by $2I_0$.

Practically, this twisted-mode scheme can be implemented using only a single quarter-wave plate as shown in Fig. 12(b). This design is possible given the small incident angle α that can be realized and the availability of commercial waveplates with retardation showing only small position and incident angle dependences (the retardation scales quadratically with the incident angle) [1,24,25].

The usage of a multi-order waveplate is advisable, as it provides a higher damage threshold compared to a single-order waveplate. Besides enabling the implementation of the twisted-mode scheme, the multi-order waveplate combined with a polarizer also acts as a birefringent filter [18,26]. The wavelength-dependent retardation in a round-trip that occurs in the four passes in the quarter-wave plate leads to a wavelength-dependent round-trip transmission $B(\lambda)$:

$$B(\lambda) = \ln\left(1 - \cos^2\left(2\pi K\frac{\lambda - \lambda_0}{\lambda_0}\right)\right), \quad \textbf{(22)}$$

where $2\pi K$ is the round-trip retardation experienced in the quarter-wave plate at the λ_0 wavelength ($K = 58$ for four passes in a 1.5 mm thick quartz plate at 1030 nm). The logarithm is used to present the transmission as coefficient of the exponential in Eq. (10).

The improved frequency selectivity achieved with the multi-order waveplate is demonstrated in Fig. 14. The black curve represents a schematic representation of the unsaturated round-trip gain G_0 of the cavity depicted in Fig. 12(b) using a thin disk made of Yb:YAG ($G_0(1030$ nm$) = 0.26$). The red curve represents the round-trip gain when accounting for the saturation effects caused by the dominant mode at $\lambda_0 = 1030$ nm. It is computed by multiplying S_{SHB} from Eq. (21) with the unsaturated gain (black curve). Because the modes located at the two maxima of this curve see a larger gain than the dominant laser mode, they will grow until their
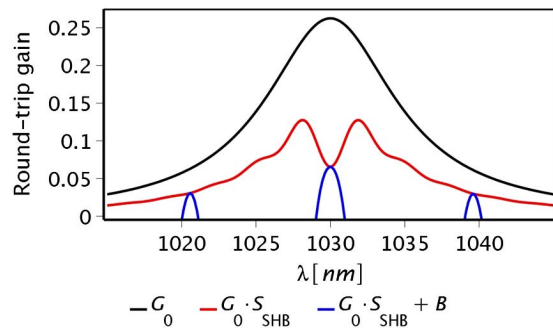
Fig. 14. Round-trip gain of the cavity depicted in Fig. 12(b) as a function of the wavelength λ. The black curve represents the unsaturated gain spectrum (we assumed a Lorentzian function as gain profile of Yb:YAG). The red curve shows the saturated gain profile for a laser operation at $\lambda_0 = 1030$ nm that accounts for SHB. We assumed $4\tau I_0/F_{\text{sat}} = 50\%$. The blue curve represents the total round-trip gain that includes the saturated gain profile and the additional losses related to the multi-order waveplate as described by Eq. (22).

saturation effects become relevant. Single-frequency operation is thus disrupted. The blue curve is the total round-trip gain that also includes the wavelength-dependent transmission $B(\lambda)$ of Eq. (22) for a quarter-wave plate based on a 1.5 mm thick quartz plate. This curve shows maximal gain for λ_0. Hence, the twisted-mode scheme can also be used for V-shaped cavities to obtain single-frequency operation.

6. DEMONSTRATION OF A *Q*-SWITCHED THIN-DISK LASER OPERATED IN TWISTED MODE

For the measurement of the 2S-2P splitting in muonic helium ions [27,28], we realized a *Q*-switched thin-disk oscillator as sketched in Fig. 15(a). The disk was used as a folding mirror, and a multi-order quarter-wave plate was inserted in front of the disk to implement the twisted-mode scheme and to provide the additional polarization-dependent losses $B(\lambda)$. The waveplate was acting also as a window for the pump module [see Fig. 15(b)], which shielded the hot front surface of the disk from air flows that would lead to optical distortions of the laser beam.

The other optical elements of the cavity, namely, the Pockels-cell (PC), a second quarter-wave plate, and a thin-film polarizer (TFP), were used to control the pre-lasing operation and the *Q*-switch dynamics as explained for a similar system in Ref. [8]. Pulses up to an energy of 110 mJ at a repetition rate of 800 Hz were delivered by the oscillator. This laser was operated flawlessly for several months at the high-intensity proton accelerator of the Paul Scherrer Institute, Villigen, Switzerland.

The effectiveness of the twisted-mode scheme in reducing SHB manifests itself also in the measured temporal profile of the emitted laser pulses. Without the quarter-wave plate, or with its axis misaligned, the SHB causes simultaneous lasing at a few longitudinal modes, resulting in mode beating with a frequency given by the round-trip time [8,30,31] [see Fig. 16 (a)]. This beating (fast oscillations) is suppressed when the quarter-wave plate is correctly aligned, as demonstrated in Fig. 16(b). The measurement of the pulse trace is thus a sensitive method to show the suppression of multi-mode operation
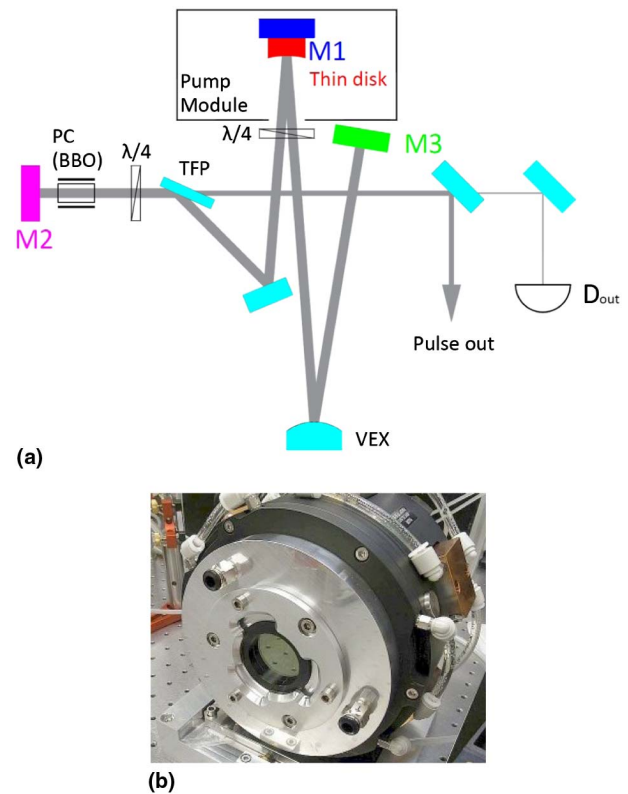
Fig. 15. (a) Scheme of the *Q*-switched thin-disk laser with twisted-mode and V-shaped layout. M2 and M3 are the end mirrors, TFP the thin film polarizer, and PC the Pockels cell. (b) Picture of the multi-order quarter-wave plate mounted to a TRUMPF pump module [29] acting also as a window.
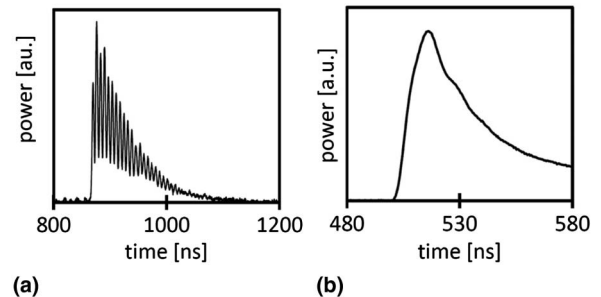
Fig. 16. Pulses emitted from the *Q*-switched thin-disk laser of Fig. 15(a); the time offsets are arbitrary. In (a), the multi-order quarter-wave plate mounted in front of the disk was rotated so that the beating is maximal. In (b), the quarter-wave plate was adjusted to produce an integer value of K that results in a suppression of the beating. Here, the pulse length is slightly shorter compared to panel (a), because during this measurement the extracted energy was larger.

[30,31]. In principle, also a spectrometer could be used, but a resolution better than 50 MHz is needed.

7. CONCLUSIONS

In this paper, we presented the wavelength-dependent decrease of the gain in an active medium caused by saturation effects.

This decrease has been expressed as $S_{SHB}(\lambda)$ for various linear-cavity layouts: simple cavity [Eq. (13) and Fig. 4], thin-disk laser with the thin disk acting as end mirror [Eq. (14) and Fig. 7], and thin-disk laser with the disk as folding mirror [Eq. (20) and Fig. 11]. We found that the spectral distance between adjacent minima and maxima in S_{SHB} around the saturating wavelength is large when the disk is used as the end mirror of the cavity. By contrast, it is small when the disk is used as a folding mirror. Hence, the "gain-at-the-end" configuration allows for easy suppression of interference effects using standard selective elements as Fabry–Perot etalons. For the more elaborate geometry where the disk acts as a folding mirror, suppression of these maxima is more challenging, given the small spectral distance (in the order of 100 MHz).

We have demonstrated that the implementation of the twisted-mode scheme in thin-disk lasers with V-shaped layouts suppresses only partially the SHB in the disk. Using the twisted-mode scheme with a multi-order waveplate, an additional wavelength-dependent loss arises that is spectrally sufficiently narrow to suppress the residual SHB effects that prevent single-frequency operation. The simplicity, efficiency, and robustness (in term of optical damage) of this scheme pave the way for achieving single-frequency operation of thin-disk lasers in the multi-kW range.

REFERENCES

1. A. Siegman, *Lasers* (University Science Books, 1986).
2. A. Mossakowska, P. Szczepański, and W. Woliński, "Influence of spatial hole burning effects on relaxation oscillations in waveguide distributed feedback Nd^{3+}:YAG lasers," Opt. Commun. **100**, 153–158 (1993).
3. K. T. Stevens, W. Schlichting, G. Foundos, A. Payne, and E. Rogers, "Promising materials for high power laser isolators," Laser Tech. J. **13**, 18–21 (2016).
4. V. Evtuhov and A. E. Siegman, "A "twisted-mode" technique for obtaining axially uniform energy density in a laser cavity," Appl. Opt. **4**, 142–143 (1965).
5. T. Kimura, K. Otsuka, and M. Saruwatari, "Spatial hole-burning effects in a Nd^{3+}:YAG laser," IEEE J. Quantum Electron. **7**, 225–230 (1971).
6. P. W. Smith, "Mode selection in lasers," Proc. IEEE **60**, 422–440 (1972).
7. Y. Park, G. Giuliani, and R. Byer, "Single axial mode operation of a Q-switched Nd:YAG oscillator by injection seeding," IEEE J. Quantum Electron. **20**, 117–125 (1984).
8. A. Antognini, K. Schuhmann, F. D. Amaro, F. Biraben, A. Dax, A. Giesen, T. Graf, T. W. Hänsch, P. Indelicato, L. Julien, C. Y. Kao, P. E. Knowles, F. Kottmann, E. L. Bigot, Y. W. Liu, L. Ludhova, N. Moschuring, F. Mulhauser, T. Nebel, F. Nez, P. Rabinowitz, C. Schwob, D. Taqqu, and R. Pohl, "Thin-disk Yb:YAG oscillator-amplifier laser, ASE, and effective Yb:YAG lifetime," IEEE J. Quantum Electron. **45**, 993–1005 (2009).
9. A. Giesen, "Thin disk lasers–power scalability and beam quality," Laser Tech. J. **2**, 42–45 (2005).
10. A. Giesen, "High-power thin-disk lasers," in *Advanced Solid-State Photonics* (Optical Society of America, 2007), paper MA1.
11. C. Vorholt and U. Wittrock, "Spatial hole burning in Yb:YAG thin-disk lasers," Appl. Phys. B **120**, 711–721 (2015).
12. R. Paschotta, J. Aus der Au, G. Spühler, S. Erhard, A. Giesen, and U. Keller, "Passive mode locking of thin-disk lasers: effects of spatial hole burning," Appl. Phys. B **72**, 267–278 (2001).
13. G. Palmer, M. Schultze, M. Siegel, M. Emons, U. Bünting, and U. Morgner, "Passively mode-locked Yb:KLu(WO^4)^2 thin-disk oscillator operated in the positive and negative dispersion regime," Opt. Lett. **33**, 1608–1610 (2008).
14. C. L. Tang, H. Statz, and G. deMars, "Spectral output and spiking behavior of solid-state lasers," J. Appl. Phys. **34**, 2289–2295 (1963).
15. D. Roess, "Analysis of a room-temperature cw ruby laser of 10 mm resonator length: the ruby laser as a thermal lens," J. Appl. Phys. **37**, 3587–3594 (1966).
16. T. Baer, "Large-amplitude fluctuations due to longitudinal mode coupling in diode-pumped intracavity-doubled Nd:YAG lasers," J. Opt. Soc. Am. B **3**, 1175–1180 (1986).
17. K. Schuhmann, A. Antognini, K. Kirch, T. Graf, M. A. Ahmed, A. Voss, and B. Weichelt, "Thin-disk laser for the measurement of the radii of the proton and the alpha-particle," in *Advanced Solid-State Lasers Congress* (Optical Society of America, 2013), paper ATu3A.46.
18. H. Walther and J. L. Hall, "Tunable dye laser with narrow spectral output," Appl. Phys. Lett. **17**, 239–242 (1970).
19. V. Magni, "Resonators for solid-state lasers with large-volume fundamental mode and high alignment stability," Appl. Opt. **25**, 107–117 (1986).
20. G. Bollen, H.-J. Kluge, K. Wallmeroth, H. W. Schaaf, and R. B. Moore, "High-power pulsed dye laser with Fourier-limited bandwidth," J. Opt. Soc. Am. B **4**, 329–336 (1987).
21. C. S. Adams, J. Vorberg, and J. Mlynek, "Single-frequency operation of a diode-pumped lanthanum-neodymium-hexaaluminate laser by using a twisted-mode cavity," Opt. Lett. **18**, 420–422 (1993).
22. H. Pan, S. Xu, and H. Zeng, "Passively Q-switched single-longitudinal-mode c-cut Nd:GdVO^4 laser with a twisted-mode cavity," Opt. Express **13**, 2755–2760 (2005).
23. Z. H. Cong, Z. J. Liu, X. Y. Zhang, Z. G. Qin, S. J. Men, Q. Fu, and H. Rao, "Actively Q-switched Nd:YAG twisted-mode cavity laser with a RTP electro-optic modulator," in *International Conference Laser Optics (LO)* (2016), paper R1-65–R1-65.
24. Edmund Optics Inc., "Understanding waveplates," (2017), https://www.edmundoptics.com/resources/application-notes/optics/understanding-waveplates/.
25. Crystech Inc., "Waveplates," (2017), http://ilphotonics.com/cdv2/Crystech-Crystals-Optics/Optics-Crystech/waveplate.pdf/.
26. M. Oka, L. Y. Liu, W. Wiechmann, N. Eguchi, and S. Kubota, "All solid-state continuous-wave frequency-quadrupled Nd:YAG laser," IEEE J. Sel. Top. Quantum Electron. **1**, 859–866 (1995).
27. A. Antognini, F. Biraben, J. M. Cardoso, D. S. Covita, L. M. Fernandes, A. L. Gouvea, T. Graf, T. W. Hänsch, M. Hildebrandt, P. Indelicato, L. Julien, K. Kirch, F. Kottmann, Y.-W. Liu, C. M. Monteiro, F. Mulhauser, T. Nebel, F. Nez, J. M. dos Santos, K. Schuhmann, D. Taqqu, J. F. Veloso, A. Voss, and R. Pohl, "Illuminating the proton radius conundrum: the µHe$^+$ lamb shift," Can. J. Phys. **89**, 47–57 (2011).
28. R. Pohl, A. Antognini, F. Nez, F. D. Amaro, F. Biraben, J. A. M. R. Cardoso, D. S. Covita, A. Dax, S. Dhawan, L. M. P. Fernandes, A. Giesen, T. Graf, T. W. Hänsch, P. Indelicato, L. Julien, C.-Y. Kao, P. Knowles, E.-O. Le Bigot, Y.-W. Liu, J. A. M. Lopes, L. Ludhova, C. M. B. Monteiro, F. Mulhauser, T. Nebel, P. Rabinowitz, J. M. F. dos Santos, L. A. Schaller, K. Schuhmann, C. Schwob, D. Taqqu, J. A. F. C. A. Veloso, and F. Kottmann, "The size of the proton," Nature **466**, 213–216 (2010).
29. TRUMPF GmbH, "Scheibenlaser," (2017), http://www.trumpflaser.com/de/produkte/festkoerperlaser/scheibenlaser/trudisk.htm.
30. A. Berry, D. Hanna, and C. Sawyers, "High power, single frequency operation of a Q-switched TEM00 Mode Nd:YAG laser," Opt. Commun. **40**, 54–58 (1981).
31. A. Caprara and J. Heritier, "Single longitudinal mode laser without seeding," U.S. patent 5,412,673 (2 May 1995).